frontiers in Energy Research

ORIGINAL RESEARCH
published: 20 January 2021
doi: 10.3389/fenrg.2020.590300

Strategies for Hydrogen-Enriched Methane Flameless Combustion in a Quasi-Industrial Furnace

Ruggero Amaduzzi[1,2], *Marco Ferrarotti*[1,2,3] *and Alessandro Parente*[1,2]*

[1]Aero-Thermo Mechanics Department, Université Libre de Bruxelles, Brussels, Belgium, [2]Université Libre de Bruxelles and Vrije Universiteit Brussel, Combustikion and Robust Optimization Group (BURN), Bruxelles, Belgium, [3]Thermal Engineering and Combustion Unit, University of Mons (UMONS), Mons, Belgium

In this present work, simulations of 20 kW furnace were carried out with hydrogen-enriched methane mixtures, to identify optimal geometrical configurations and operating conditions to operate in flameless combustion regime. The objective of this work is to show the advantages of flameless combustion for hydrogen-enriched fuels and the limits of current typical industrial designs for these mixtures. The performances of a semi-industrial combustion chamber equipped with a self-recuperative flameless burner are evaluated with increasing H_2 concentrations. For highly H_2-enriched mixtures, typical burners employed for methane appear to be inadequate to reach flameless conditions. In particular, for a typical coaxial injector configuration, an equimolar mixture of hydrogen and methane represents the limit for hydrogen enrichment. To achieve flameless conditions, different injector geometries and configuration were tested. Fuel dilution with CO_2 and H_2O was also investigated. Dilution slows the mixing process, consequently helping the transition to flameless conditions. CO_2, and H_2O are typical products of hydrogen generation processes, therefore their use in fuel dilution is convenient for industrial applications. Dilution thus allows the use of greater hydrogen percentages in the mixture.

Keywords: hydrogen, combustion, moderate or intense low-oxygen dilution combustion, flameless, furnace

OPEN ACCESS

Edited by:
Alfonso Chinnici,
University of Adelaide, Australia

Reviewed by:
Yusuf Bicer,
Hamad bin Khalifa University, Qatar
Hadi Taghavifar,
Malayer University, Iran
Manab Saha,
University of Adelaide, Australia

***Correspondence:**
Alessandro Parente
alessandro.parente@ulb.be

Specialty section:
This article was submitted to Process and Energy Systems Engineering, a section of the journal Frontiers in Energy Research

Received: *31 July 2020*
Accepted: *19 November 2020*
Published: *20 January 2021*

Citation:
Amaduzzi R, Ferrarotti M and Parente A (2021) Strategies for Hydrogen-Enriched Methane Flameless Combustion in a Quasi-Industrial Furnace. Front. Energy Res. 8:590300. doi: 10.3389/fenrg.2020.590300

1 INTRODUCTION

Moving toward carbon-neutral energy generation and consumption becomes more and more urgent, as testified by recent worldwide commitments to fight climate change such as the COP21 (UNFCCC, 2015). On the other hand, global energy consumption is expected to continue increasing and at least 60% of the world's energy will rely on combustion of bio and fossil derived fuels by 2040 (International Energy Agency, 2017). New breakthroughs in clean production and consumption of fuels are required in order to face the twofold challenge of reducing emissions and increasing demand. Renewable energy sources such as solar energy may represent an attractive solution but since they are intrinsically intermittent, they are not suited for long term energy storage. For this reason the excess energy produced by renewables can be used to synthesize energy carriers which are not fossil-derived such as hydrogen. Hydrogen is a carbon-free fuel and "globally accepted as an environmentally benign secondary form of renewable energy, alternative to fossil fuels" (Nikolaidis and Poullikkas, 2017). The production of hydrogen from renewable sources involves the use of either biomass as a feedstock or water-splitting techniques

using solar energy sources, which could become an economically viable solution in the near future (Nikolaidis and Poullikkas, 2017).

Supported by appropriate storage technologies, it is of great interest to understand whether existing systems can be retro-fitted for hydrogen combustion and it is key to develop combustion technologies that allow the consumption of sustainable fuels in a way that satisfies the requirements of thermal efficiency and low pollutant emissions. Several novel technologies have been developed in the last decades to reach this goal and they include Flameless Oxidation (Wünning and Wünning, 1997), Colorless Combustion (Arghode and Gupta, 2010), HiTAC (High Temperature Air Combustion) (Rafidi and Blasiak, 2006) and Moderate or Intense Low-oxygen Dilution (MILD) combustion (Cavaliere and de Joannon, 2004). The common feature of the aforementioned technologies is the diluted fuel charge, result of an intense mixing process, a non-visible flame and uniformly distributed reaction zone. As a result, complete and efficient combustion is usually assured, along with a very low level of noise and fluctuations, absence of soot particles and very low NO_x and CO emissions (Wünning and Wünning, 1997), (Szegö et al., 2008). Moreover, the attractiveness of these technologies derives from their fuel flexibility: the process allows the combustion of different fuels over a wide range of calorific values, from biogases (Hosseini and Mazlan, 2013; Choi and Katsuki, 2001; Colorado et al., 2010), pulverized coal (Adamczyk et al., 2017) and liquid biofuels, diesel and kerosene (Xing et al., 2017) to ammonia (Sorrentino et al., 2019), natural gas (Ferrarotti et al., 2018) and methane/hydrogen blends (Parente et al., 2008). For the sake of clarity, in the present work the authors will refer to the above-mentioned technologies as either flameless or MILD combustion interchangeably.

In the two last decades, a number of lab-scale burners have been designed in order to mimic MILD conditions. Among them, the Adelaide Jet-in-Hot-Coflow (AJHC) burner (Dally et al., 2002) and the Delft Jet-in-Hot-Coflow (DJHC) (Oldenhof et al., 2011) have received considerable attention from the combustion community, as their simplified configurations make possible the collection of the high-fidelity experimental data required for turbulent combustion models development and validation. The stand-out feature of flameless combustion is the strong interaction between chemical kinetics timescales and turbulent mixing, so that models based on scale separation between chemistry and turbulence fail in predicting the behavior of such systems (Minamoto et al., 2014). In both AJHC and DJHC MILD conditions are achieved by feeding diluted and hot streams to the coflow, directly affecting the characteristic chemical and mixing timescales of the mixture. With regards to hydrogen-enriched methane mixtures in MILD conditions, several works can be found in literature, for a wide range of reactors and lab-scale burners in various working conditions (Derudi et al., 2007; Sabia et al., 2007; Parente et al., 2008; Galletti et al., 2009; Ayoub et al., 2012). Ayoub et al. (Ayoub et al., 2012) in particular achieved flameless conditions whatever the hydrogen content for a lab-scale pilot furnace with and without air pre-heating. The main difference between the aforementioned studies and the present one relies in the size of the problem: the quasi-industrial furnace presented in this study is designed to mimic operating conditions of "real-life" systems, therefore the features of the flow field may differ significantly from those of lab-scale systems. To the authors' knowledge no similar studies on comparable systems exist in literature. In industrial systems, the distributed conditions are usually a consequence of internal aerodynamic recirculation and the modification of the local mixing timescales; these strong turbulence-chemistry interactions often prove to be a challenge for the turbulent combustion model to capture. The main issue with these industrial-scale systems however is the relative scarcity of high-fidelity experimental data, which are often limited to few operating conditions. For this reason it is important to bridge the gap between lab-scale burners and industrial systems with quasi-industrial furnaces such as the one employed for this study, as they can preserve the possibility to collect high-fidelity data while working in operating conditions which are closer to "real-life" scenarios.

The complexity of the above-mentioned MILD reaction structures have been the subject of several numerical approaches for both Reynolds Averaged Navier Stokes (RANS) (Galletti et al., 2007) and Large Eddy Simulations (LES) (Duwig et al., 2007). Reaction rate-based models have been proposed in literature and applied to MILD conditions. Among those, the Eddy Dissipation Concept (EDC) (Magnussen, 2005) and the Partially-Stirred Reactor, first proposed by Chomiak (Chomiak, 1990) and employed in the present work, can be highlighted. Both models have been employed in the past by Li et al. (Li et al., 2017; Li et al., 2018) to study the AJHC employing different definitions of the characteristic timescales. In PaSR, as in other reactor-based models, the combustion process is modeled as sequence of mixing and reaction processes in locally uniform zones. Since both the chemical and mixing timescales are explicitly taken into account, their accurate estimation is key in order to properly capture the features of the reacting structures. Among the few studies conducted concerning industrial-like systems, Ferrarotti et al. (Ferrarotti et al., 2018) investigated and provided the validation of the PaSR model of the same combustion chamber studied in this work, fed with natural gas.

The purpose of this paper is to assess the limits of the quasi-industrial furnace equipped with a flameless burner, for hydrogen-methane mixtures. A series of CFD simulations were carried out varying three main parameters: the injector geometry, the stoichiometry of the mixture and fuel dilution, and assessing when flameless conditions were reached. Three different industry-standard injector geometries were chosen. First, an overview of the PaSR model is provided, along with a brief description of the combustion chamber, then a validation of the numerical model with experimental results is presented. Lastly, the results for the various different burner configurations are discussed, in order to asses which is the most influential parameter on the burner behavior and to use the results as feedback to improve the flexibility of the furnace.

2 NUMERICAL MODELING

RANS numerical simulations were carried out with the commercial code Ansys Fluent 19.3. The mesh was generated with the software Ansys Workbench, taking advantage of the furnace symmetry when possible. The computational domain consists of an angular section of either 45 or 90° depending on the

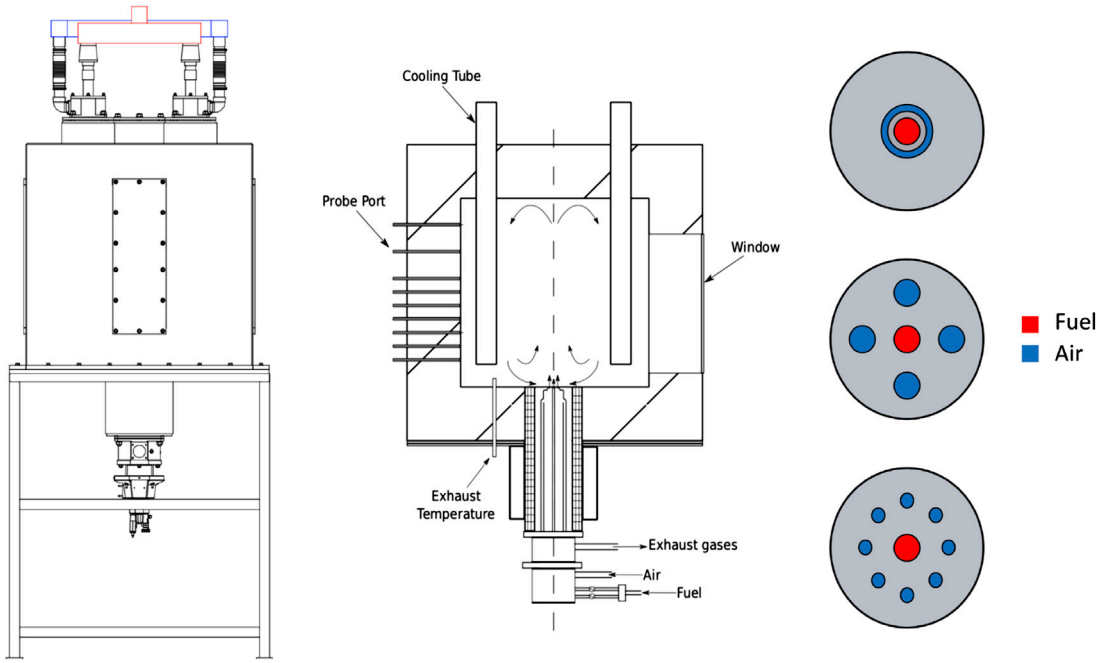

FIGURE 1 | Schematic diagram of the quasi-industrial flameless furnace: **(left)** model, **(mid)** section and **(right)** injector configurations (adapted from (Ferrarotti et al., 2020b)).

geometrical features considered for the air inlet nozzle: the former for coaxial injectors and 8-holes configurations, the latter for the 4-holes configurations. A grid convergence study was carried out and the resulting grid consists of 216 K cells for the 45° geometry and approximately twice as many for the 90° configuration. Air and fuel inlet mass flows rates were determined according to the operating conditions of each case. The fuel blends were assumed to be fed at 343 K while the air inlet temperature was determined to be 879 K after solving the energy balance across the heat exchanger. For all cases, in order to determine the heat losses associated with the cooling tubes and the furnace walls described in Section 3 the furnace outlet temeperature was set at a value of 1273 K and then the energy balance across the chamber was solved; once the heat losses were determined, a constant heat flux was set as a boundary condition for the cooling tubes and the walls of the chamber. Reynolds stresses were solved using the standard k - ε model. Radiation was taken into account using the Discrete Ordinate (DO) radiation model, using the weighted-sum-of-gray-gases (WSGG) model to account for the radiation properties of the reacting mixture, employing the coefficients proposed by (Smith et al., 1982). The interaction between turbulence and chemistry was modeled using the Partially-Stirred Reactor (PaSR) model. In the PaSR model, as in similar reactor-based models, the computational cell is split into two areas, the reaction structures and the surrounding inert fluid. The reaction progress is then determined by the exchange between the two zones. The mass fraction of the reaction region is estimated considering both the chemical and mixing timescales:

$$\kappa = \frac{\tau_c}{\tau_c + \tau_{\text{mix}}} \tag{1}$$

The mean source term for the species transport equation can be therefore expressed as:

$$\overline{\dot{\omega}} = \kappa \frac{\rho\left(Y_i^* - Y^0\right)}{\tau^*} \tag{2}$$

where ρ is the mixture density and τ^* is the residence time in the reactive region. In the original formulation proposed by Chomiak (Chomiak, 1990), the residence time was defined ashe mixing timescale τ_{mix}; in the present study τ^* is assumed as the minimum between the mixing and chemical timescales in order to account for high reactivity cases (where $\tau_c \ll \tau_{\text{mix}}$). This way, the reactants stay in the reactive structures as long as it is required. In order to estimate the mixing timescale, the so-called static approach was employed as in (Ferrarotti et al., 2018): the mixing timescale is considered as a fraction of the integral timescale k/ε by means of a constant C_{mix}:

$$\tau_{\text{mix}} = C_{\text{mix}} \frac{k}{\varepsilon} \tag{3}$$

TABLE 1 | Summary of the operating conditions for the coaxial air injector cases.

Case no	Air inlet type	ϕ_{air}	H_2%	φ
1	Coaxial	16 mm	30	0.8
2	Coaxial	16 mm	60	0.9
3	Coaxial	16 mm	5	0.8
4	Coaxial	16 mm	30	1
5	Coaxial	16 mm	50	0.8
6	Coaxial	16 mm	50	1
7	Coaxial	16 mm	70	1

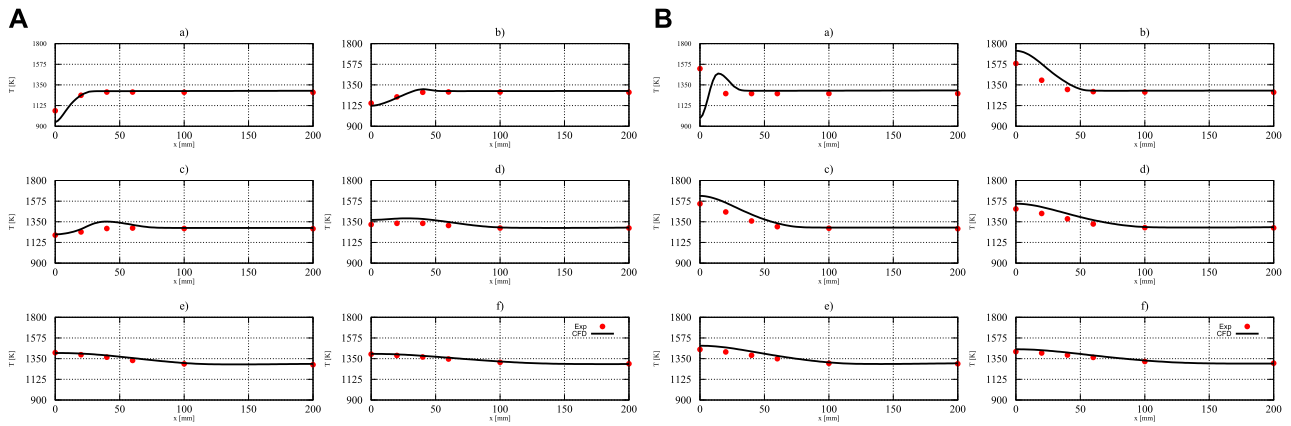

FIGURE 2 | Validation of the CFD model for cases 1 and 2 against measured temperature profiles at several axial positions: **(A)** z = 100 mm **(B)** z = 200 mm **(C)** z = 300 mm **(D)** z = 400 mm **(E)** z = 500 mm **(F)** z = 600 mm.

A value of $C_{mix} = 0.5$ was selected for all the cases considered, as it was found to be the better fit for methane MILD combustion in previous studies (Ferrarotti et al., 2018). The chemical timescale is estimated from the formation rates as the ratio between the local ith species mass fraction and its respective formation rate:

$$\tau_{c,i} = \frac{Y_i^*}{\left|dY_i^*/dt\right|} \tag{4}$$

Equation 4 refers to the characteristic timescale of a single species i. The slowest timescale among the active species is selected for the κ parameter 1) in **Eq. 2**. Li et al. (Li et al., 2018) showed that this approach is a good approximation of the chemical timescales obtained with more sophisticated and demanding techniques such as employing the eigenvalues of the Jacobian matrix of the chemical source terms. A first set of simulations was carried out in order to assess the influence of the kinetic mechanism on the results. The detailed mechanism GRI2.11 (Bowman et al., 2006) (31 species and 175 reactions) and the reduced mechanism KEE (Bilger et al., 1990) (17 species and 58 reactions) were employed.

3 FLAMELESS FURNACE DESCRIPTION AND MODEL VALIDATION

A brief description of the characteristics of the furnace employed for this study follows. A more detailed report of the features of the burner and the combustion chamber can be found in previous works (Ferrarotti et al., 2018). The quasi-industrial flameless furnace has nominal power of 20 kW. It is fired by a coaxial burner with an integrated finned heat exchanger to recover heat from the exhaust gases and to preheat the combustion air. The fuel inlet nozzle (internal diameter of 8 mm) is located at the center of the bottom wall of the furnace and it is surrounded by a coaxial air jet, for which several possible inlet nozzle configurations are possible. The furnace is equipped with four cooling tubes which allow for different stable operating conditions, in order to simulate the effects of variable loads. The fuel is fed to the burner via a feeding system composed of a set of Mass Flow Controllers for different ranges and fuels and a static mixer to create a homogeneous fuel mixture. Pure H_2O and/or CO_2 can be also fed to the mixer in order to dilute the fuel blend. A sketch of the furnace can be found in **Figure 1**.

Before performing the numerical study on hydrogen enrichment, the CFD model was validated to ensure that it provides an accurate representation of the combustion process taking place in the furnace. The CFD model employed in this work was already validated for a number of systems, including the "lab-scale" Adelaide Jet in Hot-Coflow (Li et al., 2018; Ferrarotti et al., 2020a), which is fed with a mixture of methane and hydrogen under different turbulence conditions, and the very same furnace analyzed here, fed with natural gas (Ferrarotti et al., 2018). Two reference cases were chosen to further validate the numerical model for the present study. For both cases a constant input power of 20 kW was fixed and the cooling flow rate was set in order to reach an outlet temperature of 1,000 °C. In both reference cases the geometrical features of the furnace are constant, with a fuel nozzle diameter of 8 mm and a air nozzle

TABLE 2 | Summary of the operating conditions for the multi-hole air injector cases.

Case no	Air inlet type	Air inlet tilt	Fuel inlet length	ϕ_{air}	U_{air}	H_2%
8	4-holes	No	+0 mm	9 mm	77.91 m/s	70
9	4-holes	No	+0 mm	5.4 mm	216.42 m/s	70
10	8-holes	No	+0 mm	6.4 mm	77.91 m/s	70
11	4-holes	15°	+0 mm	9 mm	77.91 m/s	70
12	4-holes	No	+100 mm	9 mm	77.91 m/s	70

TABLE 3 | Summary of the operating conditions for the diluted, coaxial injector cases.

Case no	Air inlet type	ϕ_{air}	Dilution	H_2%
13	Coaxial	16 mm	100% vol CO_2	70
14	Coaxial	16 mm	100% vol H_2O	70

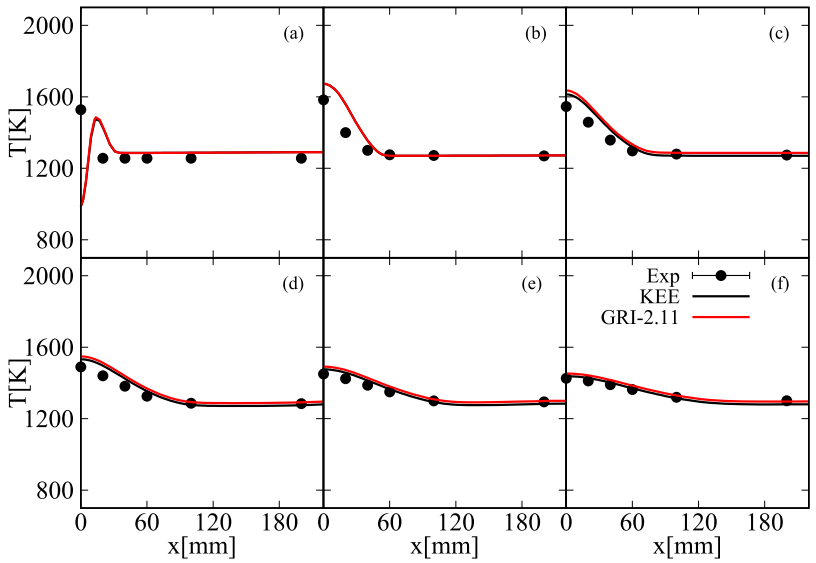

FIGURE 3 | Comparison between experimental, GRI2.11 and KEE results for case 2 at several axial locations: z = **(A)** 100 mm **(B)** 200 mm **(C)** 300 mm **(D)** 400 mm **(E)** 500 mm **(F)** 600 mm.

diameter of 16 mm. **Table 1** summarizes the operating conditions of case 1 and 2.

Figure 2 shows the CFD model results for case 1 and 2 against measured temperature profiles at several axial positions (z = 100, 200, 300, 400, 500, 600 mm). Experimental results were gathered via the use of a suction pyrometer, also described in (Ferrarotti et al., 2018). The averaged experimental uncertainty is of 10K. The numerical results well capture the measured positions, with an error below 5%. In case 1, which refers to a low hydrogen content mixture (30% in vol.), temperature profiles at all axial positions are well captured by the simulation; increasing the hydrogen content (case 2), some minor discrepancies between measured and simulated profiles at the first two axial locations (z = 100 mm and z = 200 mm) may be seen. These differences may be ascribed to a limit in RANS modeling of mixing in the reacting region of the furnace. However, performing a similar study employing LES techniques would be too computationally demanding and would therefore exceed the scope of this work.

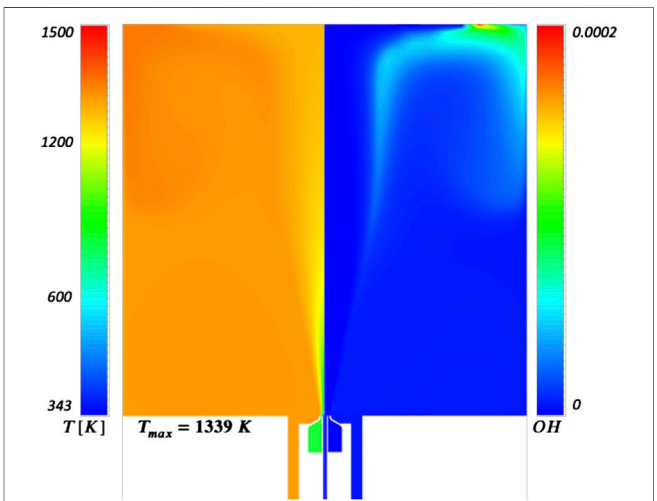

FIGURE 4 | Case 3 (5% H_2) temperature and OH contours.

4 RESULTS AND DISCUSSION

A number of different cases have been simulated in order to assess whether flameless conditions are achievable with the current burner configuration in the case of hydrogen methane enrichment. The various operating conditions are summarized in **Tables 1**–**3** sketch of the different geometrical features of the injectors is shown in **Figure 1**. As mentioned in Section 3, cases 1 and 2 were used to validate the numerical model. A comparison between two kinetic mechanisms, KEE (17 species and 58 reactions) (Bilger et al., 1990) and GRI-2.11 (31 species and 175 reactions) (Bowman et al., 2006) is represented in **Figure 3** for case 2. Being the difference between the two lower than 3%, the KEE mechanism was employed for all calculations given the lower computational cost.

Following the definition given by Cavaliere et al. in (Cavaliere and de Joannon, 2004), MILD conditions are observed when the inlet temperature is higher than the self-ignition temperature of the mixture and the overall increase of temperature due to combustion is lower than the self-ignition temperature:

$$T_{in} > T_{si} \tag{5}$$

$$\Delta T < T_{si} \tag{6}$$

Starting from case 3, it is possible to notice how typical flameless features are observed with a low hydrogen content in the mixture

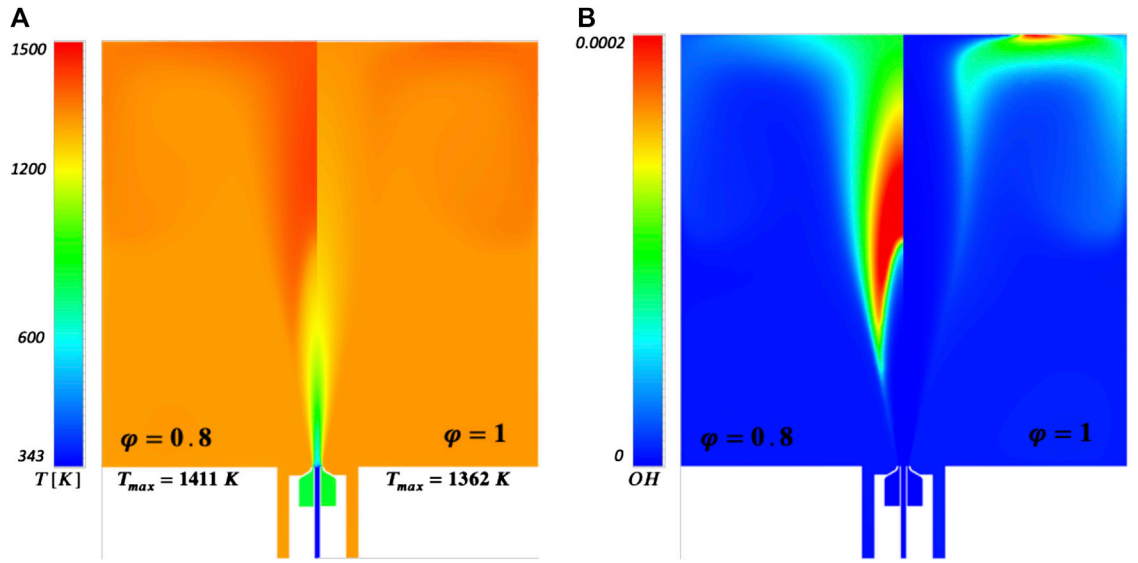

FIGURE 5 | Temperature and OH comparison for different equivalence ratio values at 30% H_2 (cases 1 and 4).

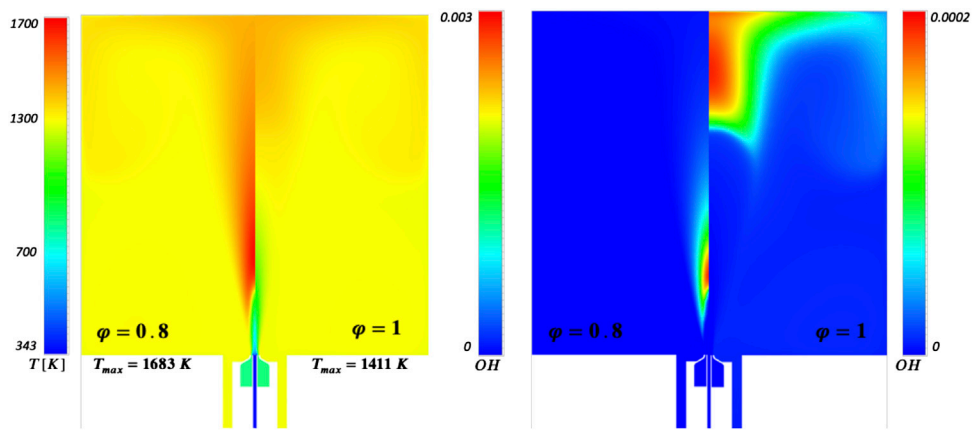

FIGURE 6 | Temperature and OH fields comparison for different equivalence ratios with 50% H_2 content (cases 5–6).

(5% in vol.). **Figure 4** shows temperature and OH contours for case 3; the temperature field is very homogeneous, with a peak temperature of 1411K and the typical delayed ignition observed with pure methane (Ferrarotti et al., 2018). Both conditions defined in **Eqs 5**, **6** are satisfied for case 3, as the temperature increase is much lower than the self-ignition temperature of the mixture of 884K. Increasing the hydrogen content to 30% in volume (cases 1 and 4), the furnace behavior starts to vary depending on the equivalence ratio φ: as one can see from both temperature and OH plots in **Figure 5a**, **5b**. With $\varphi = 0.8$ a more defined, lifted flame region appears, while in stoichiometric conditions ($\varphi = 1$, i.e. no excess air) MILD conditions are better preserved, as the temperature field is more uniform, with a peak T of 1362K against 1411K, and a delayed ignition is still observed. Nevertheless, in both cases conditions (**5**), **6**) are respected (T_{si} = 860K). Going up to 50% H_2. (cases 5 and 6), MILD conditions are still observed. **Figure 6a** shows that the maximum temperature increases by almost 300K with respect to case 4, while the OH contour in **Figure 6b** indicates how a conventional flame starts developing in these conditions: the release of OH radicals is very limited in space and its concentration is one order of magnitude higher than in previous cases. On the other hand, and perhaps counterintuitively, if $\varphi = 1$ the combustion chamber still retains a very uniform temperature field with a peak temperature of 1411K (**Figure 6a**) and a delayed ignition (**Figure 6b**). Conditions (5), 6) are satisfied for the latter case (T_{si} = 840K).

The shift toward MILD conditions and the consequent peak temperature decrease in the case of $\varphi = 1$ can be associated to an increase in the local chemical timescale near the inlet region of the furnace; this can be also observed looking at the OH contours for

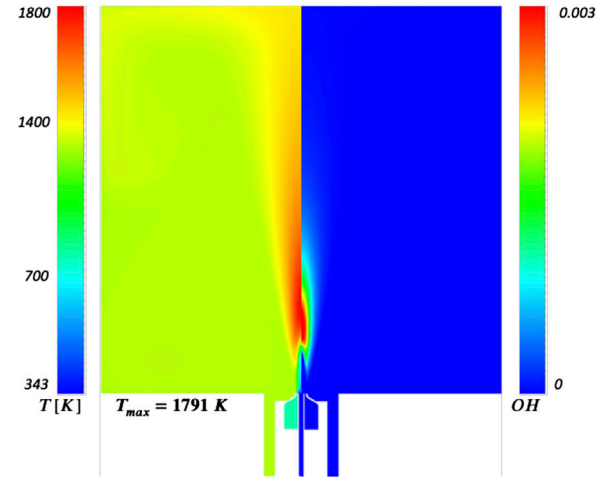

FIGURE 7 | Case 7 (70% H_2) temperature and OH contours.

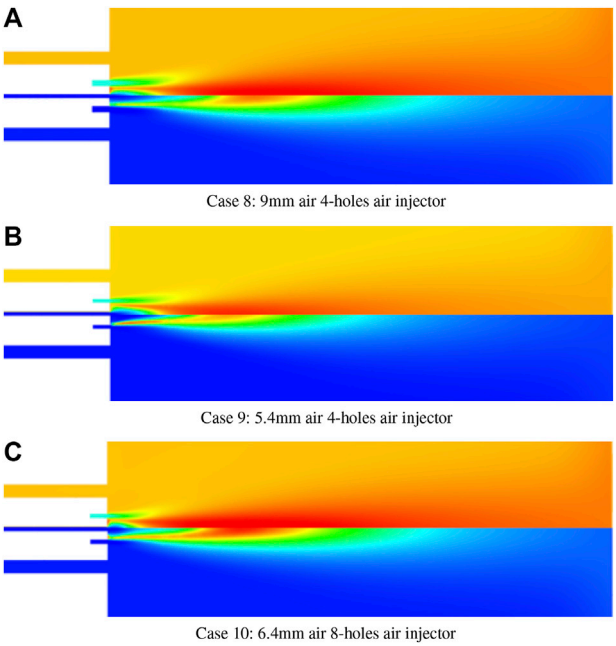

FIGURE 8 | Temperature contours for different inlet geometries with 70% H_2 content (cases 8–10).

FIGURE 9 | Case 11 (70% H_2) temperature contour. The tilting of the air inlets does not produce the desired effect.

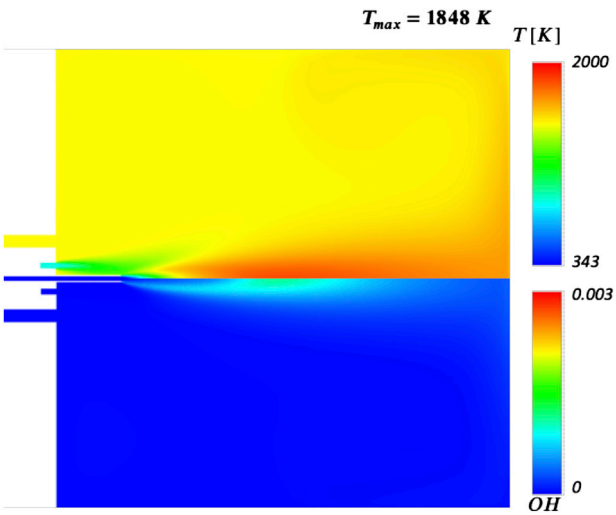

FIGURE 10 | Case 12 (70% H_2) temperature contour. The increased fuel nozzle length has the effect of reducing the maximum temperature by approximately 150 K.

φ = 0.8 and φ = 1 (6b), as in the latter case the flame lift-off is greatly increased. Increasing the equivalence ratio reduces the availability of the oxidizer at the inlet, thus increasing the time the required time for reactions to occur. This has the effect of increasing the local Damköhler number $Da = \tau_m/\tau_c$. With a hydrogen content of 70% in volume (case 7), MILD conditions are not achieved. **Figure 7** shows the typical profile of a conventional flame, with a peak temperature of 1791K.

As mentioned earlier, given the geometric configuration of the furnace, the combustion regime is a result of the combination of the turbulent mixing-chemistry interaction and the internal recirculation of the flue gases; the addition of hydrogen to the mixture results in an increased reactivity of the mixture which leads to and increase of the local Damköhler $Da \gg 1$. In order to counter balance the effect of the hydrogen enrichment, one could act on the internal recirculation and mixing in order to impact the characteristical mixing timescale and lower the local Damköhler to unity ($Da \approx 1$). For this reason, a different air inlet configuration was simulated next.

Multi-hole configuration is a typical industrial configuration for furnace inlets; cases 8 and 9 represent a 4-hole inlet with an air inlet diameter of 9 and 5.4 mm respectively while case 10 represent a 8-hole inlet with an air inlet diameter of 6.4 mm. In cases 9 and 10 the air inlet diameters were chosen in order to respectively decrease and increase the momentum flux ratio between air and fuel with respect to the coaxial configuration. The air inlet diameter in case 10 was chosen so to have the same inlet velocity as in case 8.

Figure 8a shows the temperature and OH contour plots for case 8. With respect to case 7, the peak temperature increases to 2040K and a very well defined conventional flame region forms. Increasing the air inlet velocity has no significant effect as well as one can see from **Figure 8b** (case 9). In case 10 the number of air inlets is increased to 8:

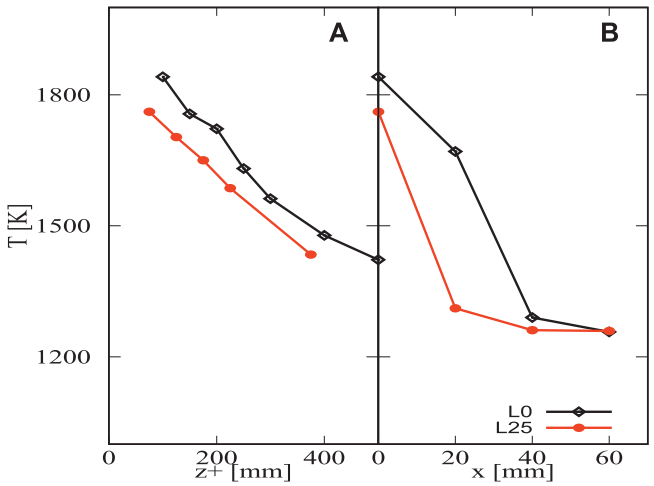

FIGURE 11 | Averaged axial and radial (z = 100 mm) temperature profiles for 75% H_2. Axial profile shown as function of z+. Averaged experimental uncertainty of 10K.

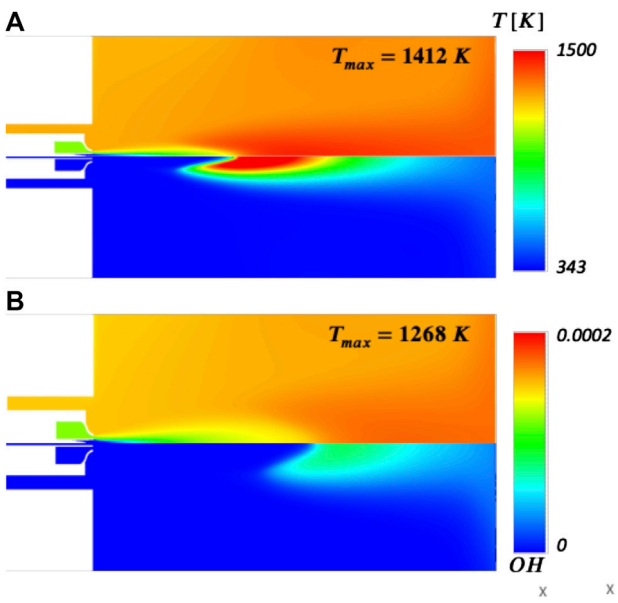

FIGURE 12 | Case 13 (a) and 14 (b) (70% H_2) temperature and OH fields. Figure **(A)** refers to dilution with 100% CO_2 in vol., figure **(B)** refers to dilution with 100% H_2O in vol.

Figure 8c shows how no significant change in the combustion regime happens in these conditions except for an increase in the maximum temperature. In an attempt to increase the mixture residence time, in case 11 the air inlets were tilted by an angle of 15 degrees. As one can see from **Figure 9** this change does not lead to a shift in the combustion regime, the only effect being a slight reduction of the peak temperature by about 50K. In order to delay the mixing, the fuel lance length was increased by 100 mm in case 12. With respect to previous cases with the 4-holes inlets, the maximum temperature is reduced by approximately 150K, but a well defined flame region is still present, as it is possible to see from **Figure 10**. As this effect is not negligible, it was investigated experimentally employing the coaxial 16 mm injector, as it appears to be the best configuration from the CFD results. In order to study the effect of the nozzle length, a different fuel lance of 25 mm is tested. **Figure 11** shows the experimental axial and radial temperature profile for a 25%/75% CH_4/H_2 mixture for the base injector and the 25 mm lance as function of the relative distance from the fuel exit (z+); the radial profile is for z= 100 mm. It is possible to observe that the 25 mm fuel lance causes a reduction of the peak temperature by almost 100 K with respect to the base injector, implying that the 25 mm one assures an adequate oxygen dilution. For this reason, the 100 mm lance employed in case 12 was not tested. For this 75% H_2 mixture, MILD conditions were achieved.

Having analyzed cases 7–12, it appears that MILD conditions with high levels of hydrogen enrichment (above 75% H_2 in vol.) are not feasible given the current burner configuration. As mentioned before, the increased reactivity caused by the hydrogen addition to the mixture strongly affects the local *Da* number, shifting the combustion regime toward mixing-controlled conditions, i.e. conventional combustion. The change of the air inlet geometrical configuration adopted in cases 7–12 does not produce the desired effect of mitigating the turbulent mixing. A similar study was performed by Ayoub et al. (Ayoub et al., 2012). The main differences between the two burners is in the combustion chamber dimensions and most importantly in the inlet configuration: in (Ayoub et al., 2012) it consists of two off-axis fuel injectors surrounding a central air jet. As a similar configuration would be impossible to replicate in the quasi-industrial flameless furnace without substituting the entire burner hardware, it was not simulated in the present work.

The last two cases analyzed (cases 13 and 14) refer to diluted fuel conditions with carbon dioxide and water respectively. Both CO_2. and H_2O are byproducts of hydrogen generating processes, therefore their employment in an industrial setting would be cost-effective. In case 13 the 30%/70% CH_4/H_2 mixture is diluted with 100% in vol. CO_2, while in case 14 the fuel is diluted with 100% H_2O is The employed air injector for both cases is the 16 mm coaxial one used in ses 1–7. **Figure 12** shows the temperature and OH contours for cases 13 and 14. In both cases, the effects of the dilution are clear: the maximum temperature is strongly reduced and the OH emissions drop by one order of magnitude. When the diluting agent is CO_2 the maximum temperature is 1412K, and a lifted flame is observable. On the other hand, H_2O dilution yields a more homogeneous temperature field and lower OH concentrations, with a further lower peak temperature of 1268K. The stronger diluting effect of water vapor may be due by its higher specific heat capacity compared to carbon dioxide, thus improving the redistribution of heat inside the furnace and consequently smoothening the temperature gradients.

5 CONCLUSION

Numerical simulations of a quasi-industrial flameless combustion chamber have been carried out with different compositions, injector geometries and dilution species in order to assess whether MILD conditions are achievable for a number of different working conditions. Numerical results were first confronted to available experimental temperature measurements at various axial locations in order to validate the CFD model.

The main findings can be summarized as follows:

- In the case of a base injector (16 mm), MILD conditions are achieved for hydrogen content up to 50% in volume depending on the equivalence ratio. More specifically, two equivalence ratios, 0.8 and 1, were tested: even at low H_2 levels (30%), MILD conditions are more easily satisfied in stoichiometric conditions and they are preserved for H_2 content up to 50%. At 70% H_2 level, a conventional flame is developed regardless of the variations of the equivalence ratio.
- Varying the injector geometry has no significant effect in the case of high H_2 contents in the mixture. Four different geometries were tested: two 4-holes configuration with different air inlet diameters (9 and 5.4 mm) in order to modify the inlet momentum flux ratio, one 8-holes air inlet (ϕ_a = 6.4 mm) and one last configuration in which the 4-holes, 9 mm air inlets are tilted by 15 degrees. In each one of the above-mentioned cases the combustion regime does not revert to flameless conditions and maximum temperatures further increase with respect to the coaxial configuration.
- Increasing the fuel nozzle length by 25 mm results in a noticeable decrease of the peak temperature; MILD conditions can be observed for up to 75% H_2 in vol.
- Fuel dilution with either CO_2. or H_2O leads to an overall smoothing of the temperature gradients in the combustion chamber, along with decreased OH emissions. In the case of CO_2 dilution the maximum temperature decreases to approximately 1400K but a conventional flame is still present. On the other hand, in the case of H_2O dilution the temperature field is more homogeneous and the peak temperature further reduces to 1268K.

In conclusion, it is more challenging to operate in MILD conditions for H_2 content higher than 50%. Increasing the fuel lance length allows to satisfy the conditions for MILD operation up to a hydrogen content of 75%. This work results suggest that different combinations of fuel inlet length and equivalence ratio φ may lead to flameless conditions in the combustion chamber for a broader range of fuel mixtures. Future works will focus on the determination of these working conditions and their experimental validation.

DATA AVAILABILIY STATEMENT

The raw data supporting the conclusions of this article will be made available by the authors, without undue reservation.

AUTHOR CONTRIBUTIONS

AP, MF, and RA have contributed to the research concept and design. RA and MF provided PaSR results. MF provided the experimental results. RA assembled the data and provided the first version of the paper along with AP. AP and MF critically revised the paper up to the final version.

FUNDING

This project has received funding from the European Research Council (ERC) under the European Union's Horizon 2020 research and innovation program under grant agreement no. 714605. The first and second authors wish to thank the Fonds de la Recherche Scientifique (FNRS) Belgium for financing their research.

REFERENCES

Adamczyk, W. P., Bialecki, R. A., Ditaranto, M., Gladysz, P., Haugen, N. E. L., Katelbach-Wozniak, A., et al. (2017). CFD modeling and thermodynamic analysis of a concept of a mild-oxy combustion large scale pulverized coal boiler. *Energy* 140, 1305–1315. doi:10.1016/j.energy.2017.03.130

Arghode, V. K., and Gupta, A. K. (2010). Effect of flow field for colorless distributed combustion (cdc) for gas turbine combustion. *Appl. Energy* 87 (5), 1631–1640. doi:10.1016/j.apenergy.2009.09.032

Ayoub, M., Rottier, C., Carpentier, S., Villermaux, C., Boukhalfa, A. M., and Honoré, D. (2012). An experimental study of mild flameless combustion of methane/hydrogen mixtures. *Int. J. Hydrogen Energy*, 37. 6912–6921. doi:10.1016/j.ijhydene.2012.01.018

Bilger, R. W., Stårner, S. H., and Kee, R. J. (1990). On reduced mechanisms for methaneair combustion in nonpremixed flames. *Combust. Flame* 80 (2), 135–149. doi:10.1016/0010-2180(90)90122-8

Cavaliere, A., and de Joannon, M. (2004). Mild combustion. *Prog. Energy Combust. Sci.* 30 (4), 329–366. doi:10.1016/j.pecs.2004.02.003

Choi, G.-M., and Katsuki, M. (2001). Advanced low nox combustion using highly preheated air. *Energy Convers. Manag.* 42 (5), 639–652. doi:10.1016/S0196-8904(00)00074-1

Chomiak, J. (1990). *Combustion a study in theory, fact and application*. Hachette, United Kingdom: Abacus Press.

Colorado, A. F., Herrera, B. A., and Amell, A. A. (2010). Performance of a flameless combustion furnace using biogas and natural gas. *Bioresour. Technol.* 101 (7), 2443–2449. doi:10.1016/j.biortech.2009.11.003

Bowman, C. T., Hanson, D. F. D., Gardiner, W. C., Lissianki, V., Smith, G. P., Golden, D. M., et al. (2006). Gri 2.11 2006.

Dally, B. B., Karpetis, A. N., and Barlow, R. S. (2002). Structure of turbulent non-premixed jet flames in a diluted hot coflow. *Proc. Combust. Inst.*, 29. 1147–1154. doi:10.1016/S1540-7489(02)80145-6

Derudi, M., Villani, A., and Rota, R. (2007). Sustainability of mild combustion of hydrogen-containing hybrid fuels. *Proc. Combust. Inst.* 31 (2), 3393–3400. doi:10.1016/j.proci.2006.08.107

Duwig, C., Stankovic, D., Fuchs, L., Li, G., and Gutmark, E. (2007). Experimental and numerical study of flameless combustion in a model gas turbine combustor. *Combust. Sci. Technol.* 180 (2), 279–295. doi:10.1080/00102200701739164

Ferrarotti, M., Amaduzzi, R., Bascherini, D., Galletti, C., and Parente, A. (2020a). Heat release rate markers for the adelaide jet in hot coflow flame. *Front. Mech. Eng.* 6 (5). doi:10.3389/fmech.2020.00005

Ferrarotti, M., Bertolino, A., Amaduzzi, R., and Parente, A. (2020b). On the Influence of Kinetic uncertainties on the accuracy of numerical modeling of an industrial flameless furnace fired with NH_3/H_2 blends: a numerical and experimental study. *Front. Energy Res.* 8:597655. doi:10.3389/fenrg.2020.597655

Ferrarotti, M., Fürst, M., Cresci, E., de Paepe, W., and Parente, A. (2018). Key modeling aspects in the simulation of a quasi-industrial 20 kW moderate or intense low-oxygen dilution combustion chamber. *Energy & Fuels* 32 (10), 10228–10241. doi:10.1021/acs.energyfuels.8b01064

Galletti, C., Parente, A., and Tognotti, L. (2007). Numerical and experimental investigation of a mild combustion burner. *Combust. Flame* 151 (4), 649–664. doi:10.1016/j.combustflame.2007.07.016

Galletti, C., Parente, A., Derudi, M., Rota, R., and Tognotti, L. (2009). Numerical and experimental analysis of no emissions from a lab-scale burner fed with hydrogen-enriched fuels and operating in mild combustion. *Int. J. Hydrogen Energy* 34 (19), 8339–8351. doi:10.1016/j.ijhydene.2009.07.095

Hosseini, S. E., and Mazlan, A. (2013). Biogas flameless combustion: a review. *Appl. Mech. Mater.* 388, 273–279. doi:10.4028/www.scientific.net/AMM.388.273

International Energy Agency (2017). *Key world energy Statistics*. Paris, France: International Energy Agency.

Li, Z., Alberto, C., Sadiki, A., and Parente, A. (2017). Comprehensive numerical study of the adelaide jet in hot-coflow burner by means of rans and detailed chemistry. *Energy* 139, 555–570. doi:10.1016/j.energy.2017.07.132

Li, Z., Ferrarotti, M., Alberto, C., and Parente, A. (2018). Finite-rate chemistry modelling of non-conventional combustion regimes using a partially-stirred reactor closure: combustion model formulation and implementation details. *Appl. Energy* 225, 637–655. doi:10.1016/j.apenergy.2018.04.085

Magnussen, B. F. (2005). "The eddy dissipation concept: a bridge between science and technology," in ECCOMAS Thematic Conference on Computational Combustion, Lisbon, Portugal, June 2005.

Minamoto, Y., Swaminathan, N., Cant, R. S., and Leung, T. (2014). Reaction zones and their structure in mild combustion. *Combust. Sci. Technol.* 186 (8), 1075–1096. doi:10.1080/00102202.2014.902814

Nikolaidis, P., and Poullikkas, A. (2017). A comparative overview of hydrogen production processes. *Renew. Sustain. Energy Rev.* 67, 597–611. doi:10.1016/j.rser.2016.09.044

Oldenhof, E., Tummers, M. J., van Veen, E. H., and Roekaerts, D. J. E. M. (2011). Role of entrainment in the stabilisation of jet-in-hot-coflow flames. *Combust. Flame* 158 (8), 1553–1563. doi:10.1016/j.combustflame.2010.12.018

Parente, A., Galletti, C., and Tognotti, L. (2008). Effect of the combustion model and kinetic mechanism on the mild combustion in an industrial burner fed with hydrogen enriched fuels. *Int. J. Hydrogen Energy* 33 (24), 7553–7564. doi:10.1016/j.ijhydene.2008.09.058

Rafidi, N., and Blasiak, W. (2006). Heat transfer characteristics of hitac heating furnace using regenerative burners. *Appl. Therm. Eng.* 26 (16), 2027–2034. doi:10.1016/j.applthermaleng.2005.12.016

Sabia, P., de Joannon, M., Fierro, S., Tregrossi, A., and Cavaliere, A. (2007). Hydrogen-enriched methane mild combustion in a well stirred reactor. *Exp. Therm. Fluid Sci.* 31 (5), 469–475. doi:10.1016/j.expthermflusci.2006.04.016

Smith, T. F., Shen, Z. F., and Friedman, J. N. (1982). Evaluation of coefficients for the weighted sum of gray gases model. *J. Heat Tran.* 104 (4), 602–608. doi:10.1115/1.3245174

Sorrentino, G., Pino, S., Bozza, P., Ragucci, R., and de Joannon, M. (2019). Low-NO_x conversion of pure ammonia in a cyclonic burner under locally diluted and preheated conditions. *Appl. Energy* 254, 113676. doi:10.1016/j.apenergy.2019.113676

Szegö, G. G., Dally, B. B., and Nathan, G. J. (2008). Scaling of NO_x emissions from a laboratory-scale mild combustion furnace. *Combust. Flame* 154 (1), 281–295. doi:10.1016/j.combustflame.2008.02.001

UNFCCC (2015). *The paris agreement*. New York, NY: UNFCCC.

Wünning, J. A., and Wünning, J. G. (1997). Flameless oxidation to reduce thermal no-formation. *Prog. Energy Combust. Sci.* 23 (1), 81–94. doi:10.1016/S0360-1285(97)00006-3

Xing, F., Kumar, A., Huang, Y., Chan, S., Ruan, C., Gu, S., and Fan, X. (2017). Flameless combustion with liquid fuel: a review focusing on fundamentals and gas turbine application. *Appl. Energy* 193, 28–51. doi:10.1016/j.apenergy.2017.02.010

Conflict of Interest: The authors declare that the research was conducted in the absence of any commercial or financial relationships that could be construed as a potential conflict of interest.